# The Structure, Energetics and Propagation of Rotating Convective Storms. Part I: Energy Exchange with the Mean Flow

DOUGLAS K. LILLY

*School of Meteorology, University of Oklahoma, Norman, OK 73019*

(Manuscript received 10 October 1984, in final form 21 August 1985)

ABSTRACT

A three-dimensional buoyant convective element responds to the existence of mean vertical shear by developing rotation about a vertical axis, with the rotational kinetic energy abstracted from that of the mean flow. This process is illustrated with the aid of linear analysis. From consideration of nonlinear processes it is concluded that a portion of the rotational energy is transformed into that of the overturning velocity field, thus enhancing further buoyant energy release. The storm structure which is optimal for energy transfer from the mean flow to rotational disturbances is a single updraft propagating with the mean flow and with counter-rotating vortices on both sides. The transfer of energy from rotational to overturning modes is, however, optimized by laterally propagating updrafts with coincident vortices.

## 1. Introduction and scope

This is the first of two articles displaying results of an investigation of the dynamics of rotating convective storms, those christened "supercells" by Browning (1964). The term "rotating convective storms" refers to the strong rotation about a vertical axis observed in these storms, but does not imply a net storm angular momentum. These articles extend the arguments earlier proposed by the author (Lilly, 1982, 1983). In them, evidence is offered that the development of rotation first amplifies and then stabilizes storm structure. The amplification mechanism, the principal subject of this paper, involves acquisition by the storm of a substantial fraction of its kinetic energy from the mean shear, with part of that energy fed back into enhancing the buoyant updraft. In Part II (Lilly, 1985; hereafter II) I show that mature quasi-steady rotating storms exhibit high flow helicity, and that this quality apparently reduces turbulence dissipation and thereby increases the efficiency and stability of the storms. The storm structure and propagation rates which maximize the buoyancy and shear energy transfers to the disturbance differ significantly from those which produce maximum updraft feedback and helicity, and I propose that the observed state represents a compromise between two limits.

Section 2 of this paper reviews the current understanding of the mechanism by which rotation and storm motion are established in supercell storms, much of that understanding being based on the results of three-dimensional numerical simulation models. Analysis of the mechanism is extended to determine the directions of the important energy transformations. In section 3, I present a linear analysis of two- and three-dimensional convection in shear, based on a technique proposed by Phillips (1966), which I believe shows more clearly than previous treatments how two-dimensionality forbids but three-dimensionality allows flow of kinetic energy from the mean state to the convective disturbance. Section 4 summarizes the results. An Appendix contains an outline of a suitable kinetic energy analysis of real and simulated storms.

## 2. Structure and motion of rotating convective storms

The discovery that certain thunderstorms, or those portions of them associated with tornadoes, contain significant rotation about a vertical axis is attributed to Brooks (1949). In seemingly unrelated work Newton and Katz (1958), from analysis of a fine-mesh raingauge network, found that many large storms moved in a direction significantly different from that of the mean flow in which they were embedded. These results, plus accumulating evidence that the most intense storms often developed in regions of strong vertical shear, were partially rationalized by Browning's (1964, 1965) model of rotating storms. Browning called these large storms supercells, in distinction to the earlier (and still accepted) model of ordinary thunderstorms as arrays of individual cells in various stages of their life cycles. Browning's model, shown schematically on Fig. 1a, b, appears as a kidney-shaped raincloud, with most of the low-level inflow and updraft occurring in the indented region and the cold downdrafts and outflow in the rain area. Looking down the mean shear vector, the motion vector of the storm is shown to the right of the mean

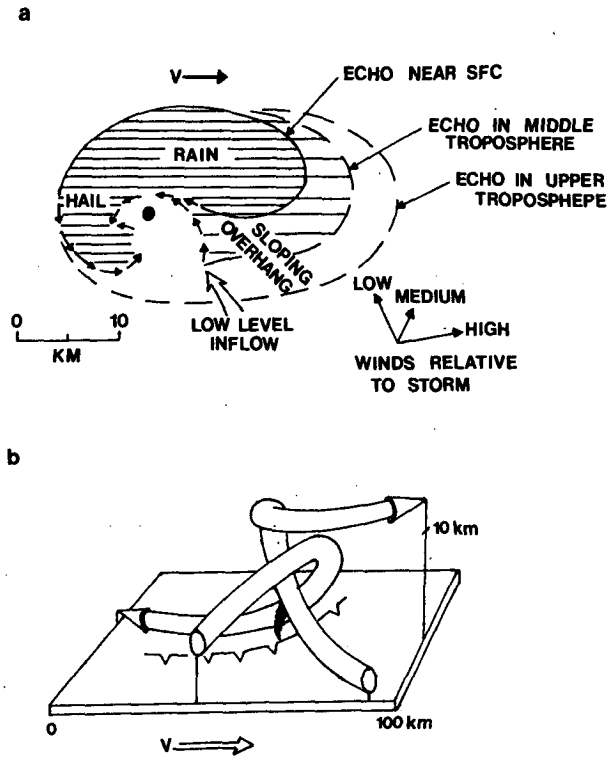


FIG. 1. (a) Horizontal sections at three levels through the radar echo of a cyclonically rotating supercell storm. Environmental winds relative to the storm in low, medium, and high levels of the troposphere are represented by the vectors L, M, and H. A typical tornado location is shown by the black circle. (b) Three-dimensional model of the airflow. Circulations are depicted relative to the storm motion. Typical positions of the surface gust front and tornado (when present) are also shown. From Browning (1964).

wind hodograph so that environmental air enters the storm (in the low levels) or passes around it (aloft) with substantial relative velocities at all levels. Cyclonic rotation of the horizontal velocity components is found in the principal updraft region, maximized at mid-levels. Air parcel trajectories involve a combination of the environmental flow and the storm-generated motions.

Browning's model, which was based on observations made using non-Doppler radar, remains accepted in most respects today, though it has been elaborated and extended in various ways, notably by Lemon and Doswell (1979). Hammond (1967) documented a storm which in many respects appeared to be a mirror image of Browning's. The storm moved to the left of the mean hodograph, i.e., faster than and to the left of the mean flow, and had radar features similar to but reversed from those of Browning's model. Storms like that which Hammond investigated are found to be in the distinct minority—about one in fifty according to Davies-Jones (1982, p. 314). Fujita and Grandoso (1968) illustrated schematically a storm "splitting" process. An initial single and apparently nonrotating storm bifurcates into two mirror-image storms diverging from each other and rotating in opposite directions. This process is frequently observed, though many supercell storms emerge without obvious splitting. A mechanism for vortex formation proposed by Browning and Landry (1963) and Barnes (1968, 1970) depends on the tilting of mean shear vorticity into the vertical by the convective updraft. The results of numerical simulation models and Doppler radar velocity measurements now confirm the Browning and Barnes mechanism and also show splitting to be a normal process for storms developing in strong unidirectional shear.

The three-dimensional convective storm simulation models developed by the NCAR-University of Illinois-NSSL group (Klemp and Wilhelmson, 1978a,b; Wilhelmson and Klemp, 1978, 1981; Klemp, Wilhelmson, and Ray, 1981; Rotunno and Klemp, 1982; Weisman and Klemp, 1982, 1984; Klemp and Rotunno, 1983) and by Clark (1979), Schlesinger (1978, 1980, 1984) and Blechman (1981) reproduce important features of the Browning-Barnes, Hammond, Fujita-Grandoso, and Lemon-Doswell results, and since the models are numerical solutions of the hydrodynamic equations, the results are accessible to detailed dynamic analysis. Such analysis has been presented by the author (Lilly, 1979, 1982, 1983), by Rotunno (1981), and most recently by Davies-Jones (1984), where a somewhat more extensive historical survey is presented.

Some aspects of the early development of a convective storm in a rectilinear shear in the lower troposphere are illustrated in Fig. 2, which is adapted from Klemp and Wilhelmson (1978a). It shows the development of the vertical and horizontal velocity fields in the shear layer for various times. An updraft is initiated by an ellipsoidal parcel of warm air rising through a conditionally unstable environment with westerly shear in the lower troposphere. In the first 30 minutes the updraft rises approximately to the tropopause. The horizontal wind at the illustrated level develops a paired vortex structure, with cyclonic rotation to the south and anticyclonic to the north of the updraft center. Over the next half hour a central downdraft, produced by rain loading and evaporative cooling, replaces the updraft and splits it laterally, with the two updraft centers moving toward the centers of rotation of the vortices. Later the downdraft also splits away from the initial buoyancy center, and the two downdrafts develop associated vorticity maxima of opposite sign to those of the updrafts. The now separate storms become approximately steady in form as they move laterally apart.

The development of rotation can be explained from consideration of the tilting terms of the vorticity equation or graphically from Fig. 3. Coriolis effects are neglected here. Klemp and Wilhelmson (1978b) found that their inclusion produced only minor changes, which is consistent with the large Rossby number of convective storms. In the first panel it is assumed that the mean shear is into the paper, so that vortex lines run from right to left. The circle represents an updraft

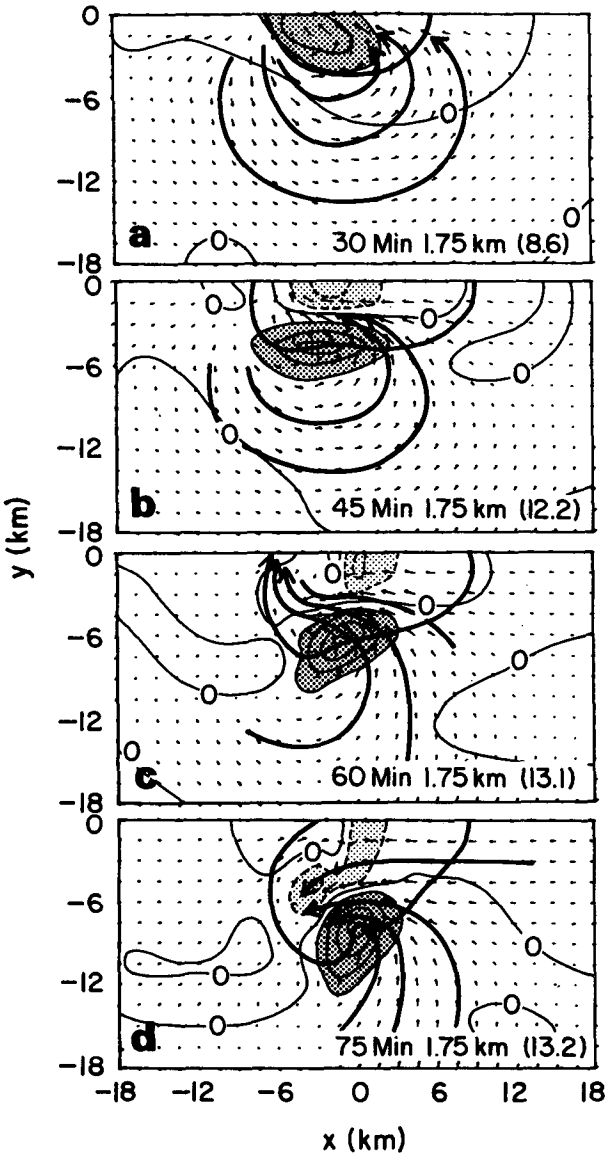


FIG. 2. Evolution of the flow field at the 1.765 km altitude in a Wilhelmson-Klemp (1978) simulation with unidirectional shear. The heavily shaded areas are updraft centers and the lightly shaded are downdraft centers. Reprinted from Lilly (1982).

region, with maximum vertical velocity in the center. The initially parallel vortex lines are tilted upward by the lateral gradient of vertical velocity, thus producing vertical components of vorticity of opposite signs to the left and right (relative to the mean shear vector) of the updraft maximum. This illustrates the situation in the first panel of Fig. 2, when the updraft is apparently being steered by the mean flow. The second panel of Fig. 3 shows the effect of an updraft on a vortex line moving through it with a velocity component parallel to the mean vorticity vector and thus normal to the mean shear vector, as is evidently occurring in Figs. 2b–d. Note that as the streamline tilts upward and then back to the horizontal plane the vortex line does the same, so that a single sign of vertical vorticity is produced, coincident with the updraft center. This second configuration differs from a similar illustration shown by Rotunno (1981, Fig. 3b), which graphically implies that the maximum vortex tilt is upstream of the maximum vertical velocity. It also differs from Davies-Jones' (1984) Fig. 7, which assumes that each lifted streamline drops back to its undisturbed position, so that each updraft vortex is associated with a downdraft vortex to its lee. I think it preferable to postulate other vortex lines becoming coincident with downdraft streamlines and producing circulation of opposite sign.

A more systematic analysis can be made from the Boussinesq equation of vertical vorticity, linearized about a mean vertical shearing flow and written in the form

$$\frac{\partial \zeta}{\partial t} + U\frac{\partial \zeta}{\partial x} = \frac{\partial U}{\partial z}\frac{\partial w}{\partial y} - \frac{\zeta}{\tau}. \tag{2.1}$$

The mean flow is taken to be unidirectional, which for the present involves no loss of generality, since the vertical disturbance structure is not being considered. The last term on the right is applied to show the qualitative effects of viscous or turbulent damping, with $\tau$ postulated as a characteristic decay time. I will use incompressible Boussinesq dynamics for nearly all conceptual analysis, in the belief that no serious qualitative discrepancies are so introduced.

Two general solutions will be discussed, corresponding to the two phases of the evolution shown on Fig. 2. For the first it is assumed that the updraft is growing exponentially, having the form

$$w = e^{\sigma t}W(x - ct, y, z)$$

where the phase speed $c$ is approximately that of the mean flow at the level where $W$ is maximized. If $\sigma$ is sufficiently large, advection terms can be ignored, at least near the level where $c = U$, and the response of (2.1) written as

$$\zeta = e^{\sigma t}\frac{\partial U}{\partial z}\frac{\partial W/\partial y}{\sigma + 1/\tau}. \tag{2.2}$$

Thus the linearized vortex tilting term produces positive and negative vertical vorticity maxima on the right and left sides, respectively, of the updraft, looking down the mean shear vector. This prediction is consistent with the flow field of Fig. 2a.

A second solution is found under the assumption that the updraft amplitude and its spatial structure are constant with time but migrate with a horizontal phase velocity $c$, which may differ from the mean flow at all levels. It now becomes convenient to express (2.1) in coordinates moving with the updraft. In such a frame, the linearized total time derivative becomes $\partial/\partial t + V\,\partial/\partial s$ where $V = |U\mathbf{i} - \mathbf{c}|$, $s = x\cos\alpha - y\sin\alpha$, and $\tan\alpha = c_y/(U - c_x)$. Equation (2.1) may then be written as

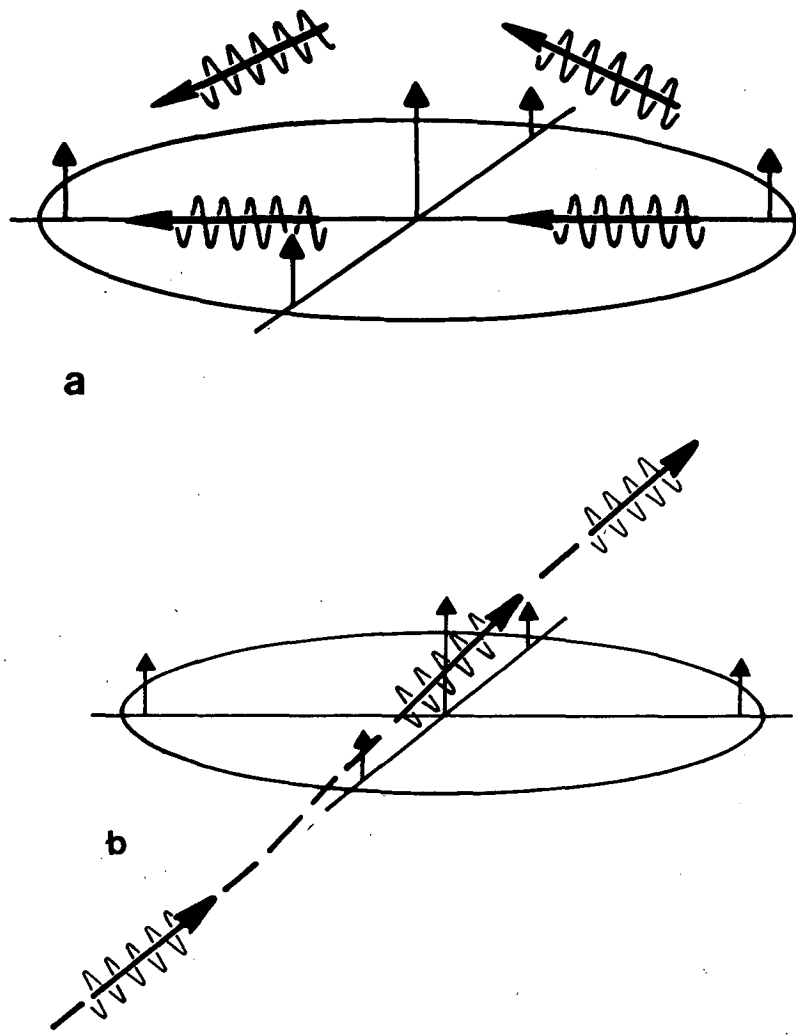


FIG. 3. Schematic illustration of tilting of vortex tubes in an updraft. In (a) the updraft is rising into a pre-existing vertical shear, directed into the paper. In (b) a mean flow moves through the updraft with its vertical shear directed from left to right and thus normal to the flow direction. Reprinted from Lilly (1982).

$$\frac{\partial \zeta}{\partial t} + V\frac{\partial \zeta}{\partial s} = \frac{\partial U}{\partial z}\frac{\partial w}{\partial y} - \frac{\zeta}{\tau}. \tag{2.3}$$

The presence of a damping term ensures that a steady state solution will eventually develop if $w$ is held constant. This solution (verifiable by differentiation) is

$$\zeta = \frac{\partial U/\partial z}{V} e^{-s/V\tau} \int_{-\infty}^{s} \frac{\partial w}{\partial y} e^{s'/V\tau} ds'. \tag{2.4}$$

Figures 4 and 5 show maps of the $\zeta$ solution, from (2.4), under the assumption that the updraft is Gaussian in its horizontal plan form, i.e.,

$$w = W_0(z)e^{-r^2/a^2},$$

$$r^2 = x^2 + y^2.$$

The critical damping factor is $V\tau/a$, the ratio of damping to advective time scales, roughly equivalent to a Reynolds number. This is set equal to either infinity or five in the figures. First, it is assumed that the updraft is moving in the $x$-direction, that is along the mean flow direction, but *slower,* so that $s = x$. The damped vorticity field, shown by the solid isolines on the lower portion of Fig. 4, is lagged and stretched out by advection but also gradually damped downstream. In the limit of zero damping, (2.4) may be written

$$\zeta = \frac{\partial U/\partial z}{V}\left(-\frac{2y}{a} W_0 e^{-y^2/a^2}\right) \int_{-\infty}^{x/a} e^{-\xi^2} d\xi.$$

Isolines of the vorticity field are shown dashed on the upper part of Fig. 4. The corresponding streamlines have not been computed but would evidently be diffluent near the updraft and leave a reduced speed wake

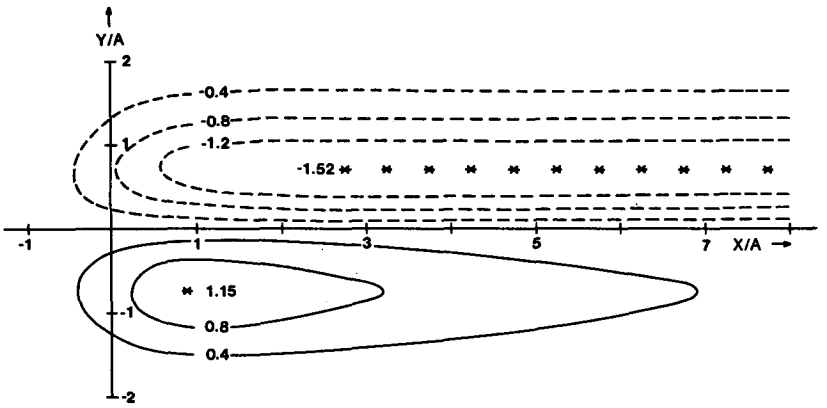


FIG. 4. Isolines of the steady state linearized vertical vorticity field produced by a mean shear flow moving through a circular updraft with a Gaussian radial profile. The mean flow and mean shear are both from the west. The lower solid isolines are for a case with Newtonian damping, and the upper isolines are for the undamped case. Each case is antisymmetric, however, with vorticity of sign opposite to $y$. The maxima are shown by asterisks, with the undamped case showing an indefinitely extended line maximum.

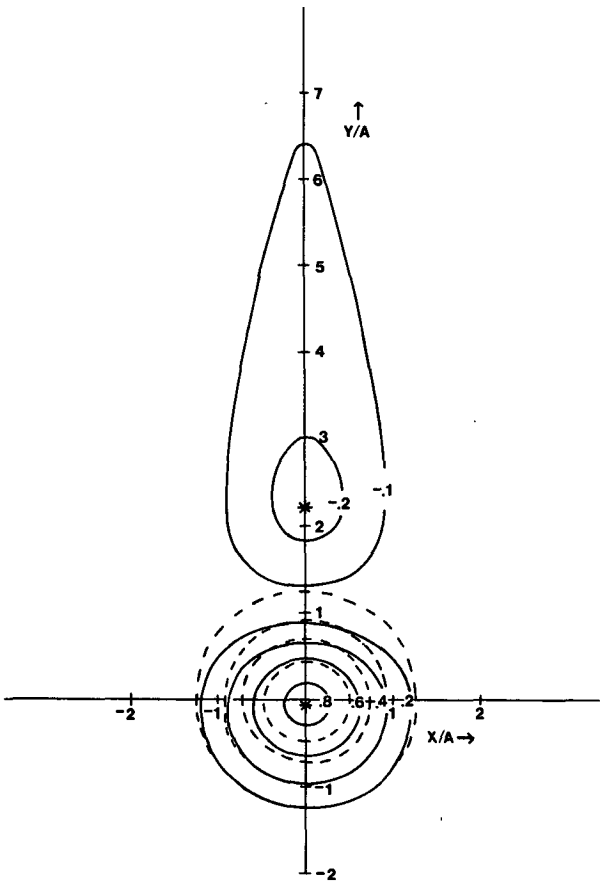


FIG. 5. As in Fig. 4 but for the mean flow direction from the south and the mean shear from the west. Solid lines correspond to the damped and dashed to the undamped flow. The undamped isolines are parallel to those of the vertical velocity field.

to the rear. This is reminiscent of the blocked flow behind a convective storm at high levels. To attain a closer similarity one would also have to incorporate the anvil outflow as a source, which would speed up the wake flow. If the updraft is assumed to move in the $x$-direction but *faster* than the mean flow, then the wake will have confluent streamlines in the updraft region. Low-level trajectories shown by Klemp, Wilhelmson and Ray (1981) tend to show such features outside the primary updraft. In both cases the horizontal velocity in the updraft is altered in the direction opposite to that of the mean shear, so that a Reynolds stress, $u'w'$, is generated with a sign opposite to $\partial U/\partial z$. This correlation will be seen to have important energetic consequences.

We next look at the laterally moving updraft. The solid isolines of Fig. 5 show the vorticity for an updraft moving to the right of the mean shear (southward), so that $s = y$ in Eq. (2.4). The velocity relative to the updraft $V$ is northward. For this case, the positive vorticity center is approximately coincident with the updraft center. The undamped version of (2.3) is $V\partial\zeta/\partial y = (\partial U/\partial z)\partial w/\partial y$ for this case, which integrates immediately to

$$\zeta = \frac{\partial U}{\partial z}\frac{w}{V}. \tag{2.6}$$

This describes a vortex which is coincident with, and proportional in amplitude to, the updraft. The isolines $\zeta$ are the dashed lines on Fig. 5. Comparison shows that the damped vorticity leads the vertical velocity a little, i.e., $\zeta_{max}$ lies slightly south of $w_{max}$. Damping also reduces the vorticity amplitude and generates a region of reversed vorticity downstream of the updraft. The

smaller the damping, the weaker but more extensive is this region, but the area integral of vorticity (circulation) is required to vanish for any finite damping. Because of the displacement of the vorticity maximum from the updraft center, the product of disturbance $u$ and $w$ velocities is again correlated negatively with the mean shear. A net Reynolds stress only exists for the damped case, however, and is much smaller here than for the updraft moving with the mean flow.

Detailed comparison of this result with Fig. 2 is probably not warranted for several reasons. The left- and right-moving circulations are not well separated in the simulations. A region of negative vorticity is present to the north of the updraft, but it is evidently produced, at least in part, by the developing downdraft.

In order to more clearly test the validity of the above analysis, I have compared the results of the laterally moving updraft model with results from model simulations. The ratio $\zeta V/(w\partial U/\partial z)$ predicted from Eq. (2.6) to be unity for inviscid flow and less with damping, was calculated at several levels from computer output data provided by M. Weisman (personal communication) for a model run similar to those presented by Weisman and Klemp (1982). The simulation was carried out on a velocity field with a shear of $7.5 \times 10^{-3}$ $s^{-1}$ at the surface, decreasing to zero above 4 km. A split pair of storms was simulated, with downstream propagation speed about equal to the mean wind at 2.5 km and a cross-shear storm motion of 6 m $s^{-1}$. The above ratio was evaluated at a time 5400 seconds after the beginning of the simulation. Table 1 shows the results. The values near the 2.5 km "steering" level show a ratio of linearly predicted to numerically simulated vorticity of about 1.5.

The moderate discrepancy between the above result and the predicted value of less than unity is apparently due to nonlinear effects. If one applies (2.6), the undamped solution, to the vorticity equation, (2.3), the unbalanced nonlinear terms are proportional to $W_0^2(d/dz)(V^{-1}dU/dz)$, and are of about the same magnitude as the linear terms. The nonlinear effect is symmetric about the vortex center, however, and thus does not qualitatively change the most important results of Eqs. (2.2) and (2.6). These are that 1) a growing updraft in a shear flow produces vortices on opposite sides of the shear vector; and 2) a steady state updraft moving laterally to the shear direction develops a single vortex coincident with the updraft.

TABLE 1. Relationship between maxima of vertical velocity and vorticity.

| $z$ (km) | $w_{max}$ (m $s^{-1}$) | $\zeta_{max}$ ($10^{-2}$ $s^{-1}$) | $V$ (m $s^{-1}$) | Ratio |
|---|---|---|---|---|
| 0.96 | 9.2 | 1.48 | 11.8 | 3.92 |
| 1.40 | 11.6 | 1.82 | 9.6 | 2.76 |
| 1.86 | 13.2 | 1.72 | 7.3 | 1.67 |
| 2.35 | 13.6 | 1.62 | 6.5 | 1.43 |
| 2.87 | 14.9 | 1.63 | 6.9 | 1.81 |
| 3.41 | 15.9 | 1.58 | 7.9 | 2.77 |
| 3.99 | 18.1 | 1.61 | 8.2 | 3.88 |

The key problem of supercell dynamics remains. Why does the updraft, after being forced out of its original position by evaporating water-loaded air, maintain its identity as a pair of laterally moving updrafts, which then direct and approximately coincide with the vortex centers? As noted by Marroquin and Raymond (1982), the Miles-Howard theorem constrains the propagation of amplifying disturbances to within the envelope formed by the mean flow hodograph, if those disturbances are controlled by linear dynamics and one ignores WAVE-CISK effects. Klemp and Rotunno (1982) use linear analysis to show that for a curved hodograph the updraft propagates with a motion vector to the inside of the hodograph curve, which seems in agreement with the Marroquin-Raymond analysis. They also show, however, that linear theory cannot account for the observed propagation of split updraft components lateral to a straight hodograph, but that the pressure field associated with finite amplitude storm-induced vortices is consistent with that propagation.

One may idealize this result by assuming that the rotary motions produced by vortex tilting are strong enough to be considered locally radially symmetric, so that $\partial/\partial\phi = 0$. Then the equation of azimuthal vorticity centered on one of these vertical vortices can be written in cylindrical coordinates as

$$\frac{d(\omega_\phi/r)}{dt} = \frac{\partial}{\partial z}(v_\phi^2/r^2) - \frac{1}{r}\frac{\partial b}{\partial r}, \tag{2.7}$$

where $v_\phi$ and $\omega_\phi$ are the azimuthal velocity and vorticity components, respectively, $\omega_\phi = \partial v_r/\partial z - \partial w/\partial r$, and $b$ is the buoyancy variable. The azimuthal vorticity is the component associated with radially symmetric overturning motions. The first term on the right generates positive vorticity below and negative above regions of rotating flow of either sign. Thus an existing updraft (or downdraft) is amplified by this effect. The last term is the buoyancy generation, which produces convective overturning when the environment is thermodynamically unstable. In the alternative approach given by Klemp and Rotunno (1982), it is assumed that a vortex develops a cyclostrophic pressure field, with a minimum at the level of maximum rotation. This reduced pressure then accelerates air upward beneath it. These two approaches are apparently equivalent, and the effect they describe could appropriately be defined as vortex suction. This terminology was first suggested by Fujita (1971) in connection with the vertical lifting of surface objects by tornadoes.

I now consider the energetic implications of the above simplified models for generation of vertical and

azimuthal vorticity. First I assume that (2.1) holds, with the implication that vertical advection and other nonlinear terms can be neglected. A kinetic energy equation for the rotational velocity $v_R$ may be constructed by multiplying (2.1) by a streamfunction $\psi$, where $v_R$ and $\psi$ are related by

$$u_R = -\partial\psi/\partial y,\ v_R = \partial\psi/\partial x,\ \zeta = \partial^2\psi/\partial x^2 + \partial^2\psi/\partial y^2.$$

Upon integrating over horizontal space and assuming the gradients of $\psi$ to be bounded at infinity, the result is

$$\frac{\partial E_R}{\partial t} = -\overline{\rho u_R w}\frac{\partial U}{\partial z} - \frac{E_R}{\tau}, \tag{2.8}$$

where $E_R = \bar{\rho}\overline{v_R^2}/2$ and the overbar denotes a horizontal average. This result shows that rotational kinetic energy is directly obtained if the product of the mean shear and the Reynolds stress exerted by the rotational velocity component is negative. The solutions to Eq. (2.1) shown in Figs. 4 and 5 both show such correlations, i.e., the westerly disturbance velocity is negatively correlated with $w$. The correlation is strong for the nonpropagating vortices in Fig. 4. For the propagating case in Fig. 5, it is produced only by the damping term.

An energy equation for the overturning (horizontally divergent plus vertical) components of the flow arises from assuming the validity of (2.7), which implies radial symmetry. Multiplication of (2.7) by another streamfunction, say $\chi$, whose Laplacian in the $r$–$z$ plane is $\omega_\phi$, leads to the result

$$r\frac{\partial E_D}{\partial t} = \bar{\rho}\overline{v_r v_\phi^2} + \bar{\rho}\overline{rwb}, \tag{2.9}$$

where

$$v_r = r^{-1}\partial\chi/\partial z,\quad w = -r^{-1}\partial\chi/\partial r,$$

$$\omega_\phi = (\partial/\partial r)(r^{-1}\partial\chi/\partial r) + r^{-1}\partial^2\chi/\partial z^2,$$

$$E_D = \bar{\rho}(\overline{v_r^2} + \overline{w^2})/2.$$

The overbar here represents a radial and vertical average, with $w$ assumed to vanish at upper and lower boundaries. The equation of azimuthal motion in a radially symmetric inviscid flow is

$$\frac{\partial v_\phi}{\partial t} + v_r\left(\frac{\partial v_\phi}{\partial r} + \frac{v_\phi}{r}\right) + w\frac{\partial v_\phi}{\partial z} = 0. \tag{2.10}$$

Multiplication by $\bar{\rho}rv_\phi$ and averaging over the $r$–$z$ plane leads to an equation for azimuthal flow energy, i.e.,

$$\frac{\partial E_\phi}{\partial t} + \bar{\rho}\overline{v_r v_\phi^2} = 0 \tag{2.11}$$

where $E_\phi = \bar{\rho}\overline{v_\phi^2}/2$. Thus if we identify $E_\phi \approx E_R$, the streamflow energy of Eq. (2.8), then $\bar{\rho}\overline{v_R v_\phi^2}$ is identified as an exchange term between rotational and overturning kinetic energy. This exchange is evidently positive if $\omega_\phi$ is being amplified by vortex suction. If $v_r$ is positive in regions of strong $v_\phi^2$, then the vortex is expanding and losing energy, but that energy must reappear in the overturning flow. I propose, therefore, that the continued lateral motion of the supercell updraft, which maintains its associated vortex by tilting of the mean flow tubes, is itself maintained by the vortex suction effect.

We recall that flow in a rotating coordinate frame, as in most large scale meteorological systems, exchanges energy between divergent and rotational components, with the transformation given by the cross-product of the rotational and divergent velocity vectors multiplied by the Coriolis parameter. The nonlinear exchange term shown between Eqs. (2.9) and (2.11) is similar, but with the Coriolis parameter replaced by $v_\phi/r$. Thus, the feedback of energy from the rotational component to the updraft may occur significantly when vorticity is large enough that the local reference frame of the updraft appears to be rotating.

The above simplified energy equations, (2.8) vs (2.9) and (2.11), are derived using different approximations and are not obviously compatible with each other. I believe that each of the simplified forms contains the essential terms which define the important energy exchange processes. The two exchanges, from mean flow to rotation and from rotation to overturning, are not optimized by the same flow field, however. As shown earlier and further illustrated in the more complete linear model of section 3, energy is transferred from the mean flow to the disturbance most effectively when a columnar updraft moves with the mean flow and vortices develop on either side of it. When the updraft moves laterally it receives only enough net energy from the mean flow to balance friction, because the mean flow passes through the disturbance and what is received in the inflow is returned in the outflow. In the real nonlinear storm the vertical velocity is sufficiently strong that this ventilation probably does not occur near the updraft maximum, so that favorable energy exchange with the mean flow could still be possible. For the nonlinear Beltrami flow idealization described in II, however, which assumes the updraft and vortex centers to coincide, again the eddy stress cancels in the horizontal average. By contrast, the transfer of energy from the rotational to the overturning components through the vortex suction mechanism is evidently maximized when the updraft and vortex coincide.

In the Appendix, a complete set of kinetic energy equations for an anelastic flow with open lateral boundaries is derived, for which the idealizations of the preceding analysis are avoided. Figure 6 depicts the kinetic energy cycle in terms of that derivation but with signs consistent with the idealized analysis. The usual route of convective energy in a nonshearing environment is shown by the processes on the upper left and middle of the diagram. Buoyant instability produces a correlation between buoyancy and vertical ve-

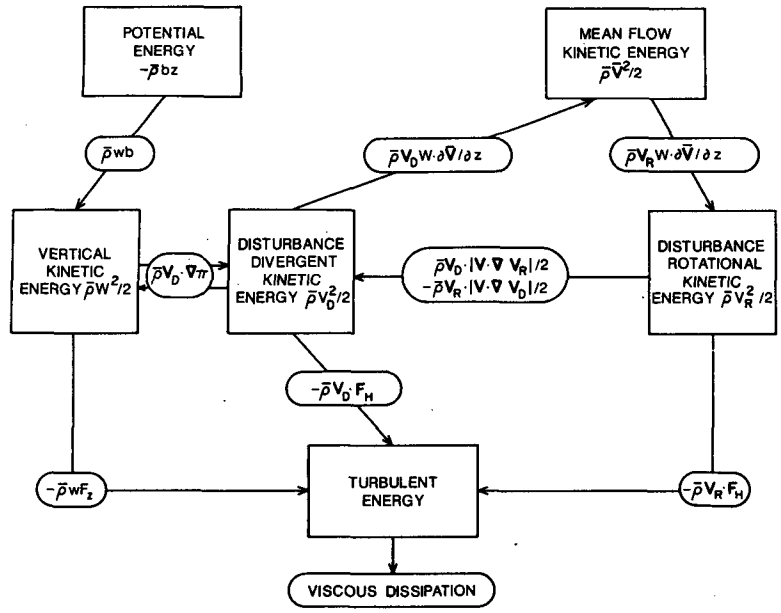


FIG. 6. The kinetic energy cycle for rotating convective storms. Sources are potential and mean flow kinetic energy, with turbulence and eventual viscous dissipation acting as the sink. Arrows are drawn in the expected direction of transfer. All exchange terms appear in Eqs. (A6), (A17), and (A18).

locity which transfers potential energy to vertical kinetic energy. Continuity and the minimization of frictional losses requires part of that vertical energy to be transferred to the disturbance energy of horizontally divergent motion. As shown in section 3, the existence of mean shear is destructive to the disturbance energy of horizontally divergent motion. Thus divergent motion energy is assumed to be transferred to mean flow energy. The rotational component, however, obtains energy from the mean flow and, as previously discussed, apparently transfers part of it to the horizontally divergent and vertical flow fields. The final branches of the energy circulation are to small-scale turbulent energy and eventual viscous dissipation.

## 3. A linear model of a buoyant element in shear

Asai (1970) utilized linear stability analysis of normal modes to show the interaction of shearing and buoyant instabilities. He found that the modes which make energy available from shear and those which utilize buoyancy are confined to different ranges of the Richardson number, and in the transition region the instability mechanisms are uncooperative, even hostile, to each other. Shearing instability modes (Kelvin–Helmholtz waves) are oriented in lines perpendicular to the mean shear, but convective instability modes with that orientation are suppressed by shear and feed part of their energy into the mean flow. The only convective modes which are not suppressed by the shear are those oriented in lines parallel to it. Such modes create disturbance energy from the shear by vertically rearranging the horizontal motion field. Those rearrangements do not interact with the vertical motions which release buoyant energy and they do not change the rate of growth of convective instabilities.

In this Section, I will show a different type of linear analysis, leading to somewhat similar results to Asai's but interpretable more directly toward the convective storm problem. The technique, due as far as I know to O. M. Phillips (1966, sec. 5.5), involves analytic time integrations of an arbitrary initial disturbance, which here takes the form of a heated column or slab. Stability is expressed as algebraic, rather than exponential, growth or decay. The purpose is to show in a simple but complete dynamical framework how two- and three-dimensional convective elements can develop different energetics, with the latter always able to extract energy from the mean flow. Emanuel (1984) has shown a rather general proof, using Miles-Howard integral techniques for two-dimensional disturbances with wave modes normal to the shear vector, that vertical momentum flux must always be up-gradient for negative static stability and a constant vertical shear in the direction of the horizontal wavenumber. Kinetic energy is then always transferred from the disturbance to the mean flow.

I assume incompressible inviscid Boussinesq dynamics, linearized about a unidirectional horizontal flow with vertical shear. The equations of motion and continuity are

$$\frac{\partial u}{\partial t} + U\frac{\partial u}{\partial x} + w\frac{dU}{dz} + \frac{\partial (p/\bar{\rho})}{\partial x} = 0, \tag{3.1}$$

$$\frac{\partial v}{\partial t} + U\frac{\partial v}{\partial x} + \frac{\partial (p/\bar{\rho})}{\partial y} = 0, \tag{3.2}$$

$$\frac{\partial w}{\partial t} + U\frac{\partial w}{\partial x} - b + \frac{\partial (p/\bar{\rho})}{\partial z} = 0, \tag{3.3}$$

$$\frac{\partial u}{\partial x} + \frac{\partial v}{\partial y} + \frac{\partial w}{\partial z} = 0. \tag{3.4}$$

The buoyancy $b$ is assumed to be conservative and linearized about a mean statically neutral state. Conservation of buoyancy is then expressed by

$$\frac{\partial b}{\partial t} + U\frac{\partial b}{\partial x} = 0. \tag{3.5}$$

The analysis is here confined to the case of a uniform shear $U = Sz$ with $S$ a constant. The domain is unbounded horizontally and vertically. An initial disturbance is postulated with the general form of a vertical slab of buoyancy, arbitrarily specified in the $x$-direction, i.e.,

$$b(x, y, z, t = 0) = b_0(x).$$

From (3.5), the solution for buoyancy may be written

$$b = b_0(\xi), \quad \xi = x - Ut = x - Stz. \tag{3.6}$$

A conservation equation for $y$-vorticity is formed by cross-differentiating (3.1) and (3.3), i.e.,

$$\frac{\partial \eta}{\partial t} + U\frac{\partial \eta}{\partial x} + \frac{\partial b}{\partial x} = 0, \tag{3.7}$$

where $\eta = \partial u/\partial z - \partial w/\partial x$. The general solution of this equation, with $b$ given by (3.6), is

$$\eta = \eta_0(\xi) - t\frac{db_0}{d\xi}.$$

If it is assumed that the initial disturbance velocity field is zero, then $\eta_0 = 0$, and

$$\eta = -t\frac{db_0}{d\xi}. \tag{3.9}$$

The two-dimensional continuity equation allows a streamfunction $\psi$ to be defined such that the velocity component and vorticity are given by

$$u = \partial\psi/\partial z, \quad w = -\partial\psi/\partial x, \quad \eta = \nabla^2\psi.$$

We transform the above into the $\xi$-coordinate by use of chain law relations, i.e.,

$$\left.\frac{\partial \psi}{\partial x}\right|_t = \frac{\partial \psi}{\partial \xi},$$

$$\left.\frac{\partial \psi}{\partial z}\right|_t = \left.\frac{\partial \xi}{\partial z}\right|_t \frac{\partial \psi}{\partial \xi} + \left.\frac{\partial \psi}{\partial z}\right|_\xi = -St\frac{\partial \psi}{\partial \xi} + \left.\frac{\partial \psi}{\partial z}\right|_\xi. \tag{3.10}$$

The possibility that $\psi$ may vary with $z$ along $\xi$ surfaces may be eliminated by the initial condition that $u = 0$ at $t = 0$. Thus, the last term of the last equality vanishes, so that

$$u = -St\partial\psi/\partial\xi, \quad w = -\partial\psi/\partial\xi,$$
$$\eta = (1 + S^2t^2)\partial^2\psi/\partial\xi^2. \tag{3.11}$$

Applying these definitions to the solution for $\eta$, (3.9) and evaluating the pressure derivative from either of the equations of motion (3.1) or (3.3) we find that

$$u = \frac{St^2}{1 + S^2t^2}b, \quad w = \frac{t}{1 + S^2t^2}b,$$
$$\frac{\partial (p/\bar{\rho})}{\partial \xi} = -\frac{St(3 + S^2t^2)}{(1 + S^2t^2)^2}b. \tag{3.12}$$

The physical interpretation of these results is fairly straightforward. The slab of buoyancy is tilted immediately and continually by the shear. It initially produces vertical velocity through buoyant acceleration, and as the slab tilts further, a horizontal velocity and pressure gradient develop. The kinetic energy and its transformations are

$$\left.\begin{aligned} \frac{u^2 + w^2}{2} &= \frac{t^2}{1 + S^2t^2}\frac{b^2}{2} \\ wb &= \frac{t}{1 + S^2t^2}b^2 \\ -\frac{dU}{dz}uw &= -\frac{S^2t^3}{(1 + S^2t^2)^2}b^2 \\ u\frac{\partial (p/\bar{\rho})}{\partial x} &= -w\frac{\partial (p/\bar{\rho})}{\partial z} \\ &= -\frac{S^2t^3}{(1 + S^2t^2)^3}(3 + S^2t^2)b^2 \end{aligned}\right\}. \tag{3.13}$$

The horizontal velocity amplitude and the kinetic energy grow monotonically but approach a steady state. The vertical kinetic energy is released by the buoyant generation term, $wb$, which reaches a maximum and then decreases like $t^{-1}$. It is transferred into horizontal kinetic energy through the pressure velocity correlation and then flows away from the disturbance into the mean flow through the eddy stress term $-uwdU/dz$, at a rate which ultimately equals that of the buoyancy generation. Referring back to Fig. 5, the two-dimensional model includes only the boxes in the upper left and middle, with energy transferred from potential to vertical to divergent horizontal and finally to mean flow kinetic forms. The eddy stress term transfers energy out of the disturbance because the disturbance streamlines are parallel to the buoyancy isolines and the product of $u$ and $w$ everywhere has the same sign as the mean shear.

The above solution also satisfies the nonlinear equations, since there is no advection of either buoyancy or vorticity by the disturbance flow. Two-dimensional solutions are probably not indefinitely stable, however. As the buoyancy isolines and streamlines are tilted downshear along constant $\xi$ surfaces, both convective and shearing instability become possible in cells developing along those surfaces, and these cells would be expected to have finite wavelengths of maximum growth. Thus, the tilted buoyancy surfaces will eventually break up into a series of convective and shearing disturbances, which produce mixing with the environment.

Solutions to (3.1)–(3.5) can also be obtained for initially columnar buoyancy disturbances, and these produce three-dimensional velocity fields. If

$$b(x, y, z, t = 0) = b_0(x, y), \tag{3.14}$$

then the general solution to (3.5) can be written

$$b = b_0(\xi, y). \tag{3.15}$$

By eliminating $u$, $v$, and $p$ from Eqs. (3.1)–(3.4), a relation between $w$ and $b$ is obtained, i.e.,

$$\left(\frac{\partial}{\partial t} + U\frac{\partial}{\partial x}\right)\nabla^2 w = \nabla_H{}^2 b,$$

where $\nabla_H{}^2 = \partial^2/\partial\xi^2 + \partial^2/\partial y^2$. If we make a similar assumption to that used to obtain (3.9), time becomes a parameter and we are left with a spatial elliptic partial differential equation to integrate, written in $\xi$, $y$ coordinates as

$$(1 + S^2t^2)\frac{\partial^2 w}{\partial\xi^2} + \frac{\partial^2 w}{\partial y^2} = t\left(\frac{\partial^2}{\partial\xi^2} + \frac{\partial^2}{\partial y^2}\right)b_0(\xi, y). \tag{3.16}$$

A vertical vorticity equation is now derived by cross-differentiating (1) and (2), i.e.,

$$\frac{\partial\zeta}{\partial t} + U\frac{\partial\zeta}{\partial x} = S\frac{\partial w}{\partial y}, \tag{3.17}$$

from which $\zeta$ can be similarly solved after (3.16) is solved for $w$.

To find a more explicit solution, it is convenient to consider the contribution from a single Fourier mode. I assume, therefore, that

$$b_0(x, y) = B\cos kx\cos ly. \tag{3.18}$$

This corresponds to a checkerboard pattern of alternate positively and negatively buoyant columns. Complete flow solutions are now easily found in the form

$$b = B\cos k\xi\cos ly,\ w = (\kappa_H{}^2/\kappa^2)tb, \tag{3.19}$$

$$u = \left[\frac{k^2St^2}{\kappa^2} - \frac{l^2}{k^2S}\ln\left(\frac{\kappa}{\kappa_H}\right)\right]b,$$

$$v = -\left[\frac{klSt^2}{\kappa^2} + \frac{l}{kS}\ln\left(\frac{\kappa}{\kappa_H}\right)\right]B\sin k\xi\sin ly,$$

$$\frac{\partial(p/\bar{\rho})}{\partial\xi} = -\left(1 + \frac{2\kappa_H{}^2}{\kappa^2}\right)\frac{k^2St}{\kappa^2}b,$$

$$\frac{\partial(p/\bar{\rho})}{\partial y} = \left(1 + \frac{2\kappa_H{}^2}{\kappa^2}\right)\frac{klSt}{\kappa^2}B\sin k\xi\sin ly,$$

where $\kappa_H{}^2 = k^2 + l^2$, $\kappa^2 = k^2(1 + S^2t^2) + l^2$.

Comparison with (3.12) shows that the above expressions for $b$, $w$, and $p$ are fairly similar to those for the two-dimensional case except for the $y$-variability and wavenumber and for the addition of new terms in the horizontal velocity solutions. The first terms of $u$ and $v$ are divergent and irrotational, and are similar to the horizontal velocity in the two-dimensional case. They acquire energy from the vertical component through pressure-velocity correlations, and the $u$-component returns it to the mean flow through the eddy stress. As with the two-dimensional terms, they eventually attain a steady amplitude, since the limit as $t \to \infty$ of $k^2St^2/\kappa^2 = S^{-1}$. The second horizontal velocity terms are rotational and non-divergent, and arise from the vortex tilting process. The $u$-component acquires energy from the mean flow and transmits some of it to the $v$-component through the same mechanism which produced Fig. 4. Both rotational velocity components grow logarithmically with time and, since the $u$-component is negatively correlated with $w$, the net eddy stress becomes downgradient. These results are consistent with transfer of energy from the mean flow to the disturbance kinetic energy as shown on Fig. 5. Because the velocity vectors and buoyancy isolines are no longer parallel, the linear flow solutions do not satisfy the nonlinear equations of motion or buoyancy conservation for this case.

An interesting, though possibly misleading, aspect of the linear analysis is the apparent demonstration that the tilt of an updraft is not related to its momentum flux or kinetic energy exchange with the mean flow. Although the three-dimensional disturbance tilts at the same rate as does the two-dimensional disturbance, the three-dimensional disturbance $u$-component becomes reversed in direction from that of the two-dimensional disturbance, because $wdU/dz$ exceeds $\partial(p/\bar{\rho})/\partial x$ in the horizontal equation of motion. A nonlinear solution would probably not, however, allow many streamlines to cross through the buoyant column, leading presumably to a more upright or even upshear-tilted column. Such a result has been demonstrated by Schlesinger (1984) in a comparison of two-dimensional and three-dimensional simulations of moist convection in a simple shear profile.

## 4. Summary and outlook

The principal message I have tried to convey herein is contained in the directions of the arrows on Fig. 5 linking the mean flow and disturbance kinetic energies, and in the implications of these linkages to storm

structure and propagation. The accepted wisdom that two-dimensional buoyant elements give up energy to a mean shearing flow has been extended, at least in the linear case, to the overturning flow component of three-dimensional elements. A transfer in the reverse direction is found to be associated with the development of a flow component with rotation about a vertical axis. This transfer is maximized when the convective element is moving with the mean flow at some level (or all levels). The important result yet to be proven is that rotational energy is transferred to divergent horizontal and then to vertical energy, where it can enhance the buoyant energy release. The existence of this transfer seems both a necessary consequence and a cause of the observed close correlations between updraft and vortex locations and movements. Partial energy budget calculations from model simulations have been carried out and will be presented in a subsequent paper.

*Acknowledgments.* Discussion with numerous colleagues, particularly R. Rotunno, M. Weisman, and K. Emanuel have helped clarify my thinking. In particular Rotunno pointed out the Phillips analysis used in section 3. This work was supported by the National Science Foundation's Atmospheric Science Division Grant ATM 8300603.

## APPENDIX

### Kinetic Energy Budget Analysis of an Anelastic System with Open Boundaries

This is presented for reference within the body of this paper and in future energy budget studies. In contrast to earlier cloud models, the Klemp-Wilhelmson and most other current storm simulation models have open lateral boundaries and no constraint on mean vertical velocities. In addition, for our purposes it is desirable to decompose the disturbance horizontal kinetic energy into rotational and divergent components.

The anelastic vector equation of horizontal motion is given by

$$\frac{\partial \mathbf{V}_H}{\partial t} + \nabla \cdot \nabla \mathbf{V}_H + \nabla_H \pi = \mathbf{F}_H, \tag{A1}$$

where $\pi = c_p\theta_0\{(p/p_0)^{R/c_p} - (\bar{p}/p_0)^{R/c_p}\}$, with $\theta_0$ a reference potential temperature, $p_0$ a reference surface pressure and $\bar{p}$ a mean state pressure in hydrostatic equilibrium with the reference atmosphere. The equation of vertical motion is

$$\frac{\partial w}{\partial t} + \mathbf{V} \cdot \nabla w + \frac{\partial \pi}{\partial z} - b = F_z, \tag{A2}$$

where $b$ is a buoyancy deviation from the reference state, typically given by

$$b = g(T_v - \bar{T}_v)/\bar{T}_v \tag{A3}$$

with $T_v$ a virtual temperature, including effects of vapor and liquid water density. The anelastic continuity equation is

$$\nabla \cdot (\bar{\rho}\mathbf{V}) = 0 \tag{A4}$$

where $\bar{\rho} = (p_0/R\theta_0)(\bar{p}/p_0)^{c_v/c_p}$, the mean density of the reference atmosphere.

A mean horizontal kinetic energy is formed by dot-multiplying (A1) by $\bar{\rho}\mathbf{V}_H$ and averaging over the horizontal area of interest, i.e.,

$$\bar{\rho}\frac{\partial(\overline{V_H^2/2})}{\partial t} + \frac{\bar{\rho}}{A}\oint v_n \frac{V_H^2}{2}\,ds + \frac{\partial}{\partial z}\left(\bar{\rho}\,\overline{w\frac{V_H^2}{2}}\right) + \frac{\bar{\rho}}{A}\oint v_n \pi ds - \bar{\rho}\overline{\pi \nabla_H \cdot \mathbf{V}_H} = \bar{\rho}\overline{\mathbf{V}_H \cdot \mathbf{F}_H} \tag{A5}$$

where $\bar{(\ )} = A^{-1}\iint (\ )dxdy$, $A = \iint dxdy$, $\oint (\ )ds$ is the line integral of $(\ )$ around the perimeter of the area $A$, and $v_n$ is the velocity component normal to that perimeter. The mean vertical kinetic energy equation is

$$\bar{\rho}\frac{\partial(\overline{w^2/2})}{\partial t} + \frac{\bar{\rho}}{A}\oint v_n \frac{w^2}{2}\,ds + \frac{\partial}{\partial z}\left(\bar{\rho}\,\overline{\frac{w^3}{2}}\right) + \bar{\rho}\overline{w\frac{\partial \pi}{\partial z}} - \bar{\rho}\overline{wb} = \bar{\rho}\overline{wF_z}. \tag{A6}$$

Note that the last term on the left of (A5) added to the next to last on the left of (A6) leaves a vertical pressure flux as a remainder. These terms therefore represent the exchange of energy between vertical and horizontal components.

In order to form the equations for kinetic energy of the mean and disturbance flows separately, we first obtain the mean momentum and continuity equations. Equation (A1) is multiplied by mean density, combined with (A4) and averaged to yield the mean horizontal momentum equation in the form

$$\bar{\rho}\frac{\partial \bar{\mathbf{V}}_H}{\partial t} + \frac{\bar{\rho}}{A}\oint v_n \mathbf{V}_H ds + \frac{\partial}{\partial z}[\bar{\rho}(\bar{w}\bar{\mathbf{V}}_H + \overline{w'\mathbf{V}'_H})] + \frac{\bar{\rho}}{A}\oint \mathbf{i}_n \pi ds = \bar{\rho}\bar{\mathbf{F}}_H. \tag{A7}$$

Equation (A2) is treated similarly to derive the mean vertical momentum equation, i.e.,

$$\bar{\rho}\frac{\partial \bar{w}}{\partial t} + \frac{\bar{\rho}}{A}\oint v_n w ds + \frac{\partial}{\partial z}\bar{\rho}(\bar{w}^2 + \overline{w'^2}) + \frac{\partial \bar{\pi}}{\partial z} - \bar{b} = \bar{\rho}\bar{F}_z \tag{A8}$$

where $(\ )' = (\ ) - \bar{(\ )}$, $\mathbf{i}_n$ is the unit vector normal to the boundary, and the Reynolds postulates are assumed. The mean continuity equation is obtained by taking the average of (A4) to yield

$$\frac{\bar{\rho}}{A}\oint v_n ds + \frac{\partial}{\partial z}(\bar{\rho}\bar{w}) = 0. \tag{A9}$$

The mean flow kinetic energy equations are now obtained by multiplying (A7) by $\bar{\mathbf{V}}_H$ and (A8) by $\bar{w}$ and rearranging the second and third terms with the aid of (A9):

$$\bar{\rho}\frac{\partial \bar{V}_H^2/2}{\partial t}+\frac{\bar{\rho}}{A}\oint v_n(\bar{V}_H^2/2+\bar{\mathbf{V}}_H\cdot\mathbf{V}'_H)ds+\frac{\partial}{\partial z}[\bar{\rho}(\bar{w}\bar{V}_H^2+\overline{w'\mathbf{V}'_H}\cdot\bar{\mathbf{V}}_H)]-\bar{\rho}\overline{w'\mathbf{V}'_H}\cdot\frac{\partial \mathbf{V}_H}{\partial z}+\frac{\bar{\rho}}{A}\oint \bar{v}_n\pi ds=\bar{\rho}\bar{\mathbf{V}}_H\cdot\bar{\mathbf{F}}_H, \tag{A10}$$

$$\bar{\rho}\frac{\partial \bar{w}^2/2}{\partial t}+\frac{\bar{\rho}}{A}\oint v_n(\bar{w}^2/2+\bar{w}w')ds+\frac{\partial}{\partial z}\left[\bar{\rho}\bar{w}\left(\frac{\bar{w}^2}{2}+\frac{\overline{w'^2}}{2}\right)\right]-\bar{\rho}\overline{w'^2}\frac{\partial \bar{w}}{\partial z}+\bar{\rho}\bar{w}\frac{\partial \bar{\pi}}{\partial z}-\bar{\rho}\bar{w}\bar{b}=\bar{\rho}\bar{w}\bar{F}_z. \tag{A11}$$

The disturbance energy equations are obtained by subtracting (A10) from (A5) and (A11) from (A6), yielding

$$\bar{\rho}\frac{\partial}{\partial t}(\overline{V'^2_H}/2)+\frac{\bar{\rho}}{A}\oint v_n(V'^2_H/2)ds+\frac{\partial}{\partial z}(\bar{\rho}\overline{wV'^2_H}/2)+\bar{\rho}\overline{w'\mathbf{V}'_H}\cdot\partial\bar{\mathbf{V}}_H/\partial z+\frac{\bar{\rho}}{A}\oint v'_n\pi' ds-\bar{\rho}\overline{\pi'\nabla_H\cdot\mathbf{V}'_H}=\bar{\rho}\overline{\mathbf{V}'_H\cdot\mathbf{F}'_H}, \tag{A12}$$

$$\bar{\rho}\frac{\partial}{\partial t}\left(\frac{\overline{w'^2}}{2}\right)+\frac{\bar{\rho}}{A}\oint v_n\frac{w'^2}{2}ds+\frac{\partial}{\partial z}\left(\bar{\rho}\overline{w\frac{w'^2}{2}}\right)+\bar{\rho}\overline{w'^2}\frac{\partial \bar{w}}{\partial z}+\bar{\rho}\overline{w'\frac{\partial \pi}{\partial z}}-\bar{\rho}\overline{w'b'}=\bar{\rho}\overline{w'F'_z}. \tag{A13}$$

Finally, we wish to separately consider the disturbance energy associated with horizontally nondivergent and irrotational flow components. We let

$$\mathbf{V}'_H=\mathbf{V}_R+\mathbf{V}_D,$$

with

$$\mathbf{V}_R=\mathbf{k}\times\nabla_H\psi,\quad \mathbf{V}_D=\nabla_H\phi, \tag{A14}$$

where the streamfunction $\psi(x, y, z)$ and potential function $\phi(x, y, z)$ are determined from solutions of the horizontal Poisson equations

$$\nabla_H^2\psi=\zeta,\quad \nabla_H^2\phi=\nabla_H\cdot\mathbf{V}_H. \tag{A15}$$

The decomposition of kinetic energy between horizontally nondivergent and irrotational components is not unique if the spatial domain is finite. A portion of the velocity field, which contains neither vorticity nor divergence, and depends entirely on the velocities at the other boundary, may be assigned arbitrarily to either the stream or potential flow. The average horizontal kinetic energy $\overline{V'^2}=\overline{V_R{}^2}+\overline{V_D{}^2}+2\overline{V_RV_D}$. The latter term need not vanish, but can be written as a line integral around the domain, i.e.,

$$\overline{V_RV_D}=\frac{1}{A}\int\int V_RV_Ddxdy=\frac{1}{A}\oint\psi d\phi=-\frac{1}{A}\oint\phi d\psi \tag{A16}$$

where $A$ is the area of the domain. The further the boundaries are from the principal vorticity and divergence centering regions, the smaller this term becomes.

The kinetic energy equations for the non-divergent and irrotational components can be obtained by multiplying (A1) by $\mathbf{V}_R$ and $\mathbf{V}_D$, respectively. After averaging over horizontal space, these may be written

$$\bar{\rho}\frac{\partial}{\partial t}\left(\frac{\overline{\mathbf{V}_R^2}}{2}\right)+\frac{\partial}{\partial z}\left(\bar{\rho}\frac{\overline{wV_R^2}}{2}\right)+\bar{\rho}\overline{\mathbf{V}_Rw'}\cdot\frac{\partial\bar{\mathbf{V}}_H}{\partial z}+\frac{\rho}{2}\overline{[\mathbf{V}_R\cdot(\mathbf{V}\cdot\nabla\mathbf{V}_D)-\mathbf{V}_D\cdot(\mathbf{V}\cdot\nabla\mathbf{V}_R)]}-\bar{\rho}\overline{\mathbf{V}_R\cdot\mathbf{F}_H}$$
$$=\bar{\rho}\overline{\nabla_H\cdot\left[\psi\mathbf{k}\times\left(\frac{\partial\mathbf{V}_R}{\partial t}+\mathbf{V}\cdot\nabla\mathbf{V}_H-\mathbf{F}_H\right)-\mathbf{V}_H\left(\frac{\mathbf{V}_R\cdot\mathbf{V}_D}{2}\right)\right]}, \tag{A17}$$

$$\bar{\rho}\frac{\partial}{\partial t}\left(\frac{\overline{\mathbf{V}_D^2}}{2}\right)+\frac{\partial}{\partial z}\left(\bar{\rho}\frac{\overline{wV_D^2}}{2}\right)+\bar{\rho}\overline{\mathbf{V}_Dw'}\cdot\frac{\partial\mathbf{V}_H}{\partial z}-\frac{\bar{\rho}}{2}\overline{[\mathbf{V}_R\cdot(\mathbf{V}\cdot\nabla\mathbf{V}_D)-\mathbf{V}_D\cdot(\mathbf{V}\cdot\nabla\mathbf{V}_R)]}+\bar{\rho}\overline{\mathbf{V}_D\cdot\nabla_H\pi}-\bar{\rho}\overline{\mathbf{V}_D\cdot\mathbf{F}_H}$$
$$=\bar{\rho}\overline{\nabla_H\cdot\left[\phi\left(\frac{\partial\mathbf{V}_D}{\partial t}+\mathbf{V}\cdot\nabla\mathbf{V}_H+\nabla_H\pi-\mathbf{F}_H\right)+\mathbf{V}_H\left(\frac{\mathbf{V}_R\cdot\mathbf{V}_D}{2}\right)\right]}. \tag{A18}$$

The terms which depend explicitly on the lateral boundaries have been placed on the right-hand side. These can be evaluated, and if found sufficiently small the ambiguity may be regarded as unimportant.

Comparison of the above relations to the total disturbance energy equation, (A12), shows that the first, second and third terms of (A17) and (A18) are similar to, and sum approximately to, the first, third and fourth of (A12). The pressure-velocity correlation terms in (A12) only appear in the divergent energy equation, (A18), showing that divergent energy exchanges directly with the vertical kinetic energy. The bracketed terms on the left-hand side of (A17) and (A18) show the new and unique aspect of this decomposition, as they represent an exchange between the irrotational and nondivergent kinetic energies.

## REFERENCES


Asai, T., 1970: Stability of a plane parallel flow with variable vertical shear and unstable stratification. *J. Meteor. Soc. Japan,* **48,** 129–138.

Barnes, S. L., 1968: On the source of thunderstorm rotation. ESSA Tech. Memo NSSL 38. National Severe Storms Laboratory, Norman, OK.

——, 1970: Some aspects of a severe right-moving thunderstorm deduced from mesonetwork observations. *J. Atmos. Sci.,* **27,** 634–648.

Blechman, J. B., 1981: Vortex generation in a numerical thunderstorm model. *Mon. Wea. Rev.,* **109,** 1061–1071.

Brooks, E. M., 1949: The tornado cyclone. *Weatherwise,* **2,** 32–33.

Browning, K. A., 1964: Airflow and precipitation trajectories within severe local storms which travel to the right of the winds. *J. Atmos. Sci.,* **21,** 634–639.

——, 1965: The evolution of tornadic storms. *J. Atmos. Sci.,* **22,** 664–668.

——, and C. R. Landry, 1963: Airflow within a tornadic storm. *Preprints, 10th Weather Radar Conference,* Amer. Meteor. Soc., 116–122.

Clark, T. L., 1979: Numerical simulation with a three-dimensional cloud model: Lateral boundary condition experiments and multicellular severe storm simulation. *J. Atmos. Sci.,* **36,** 2191–2215.

Davies-Jones, R. P., 1982: Tornado Dynamics. *Thunderstorms, Vol. 2, Thunderstorm Morphology and Dynamics,* E. Kessler, Ed., U.S. Dept. of Commerce, NOAA, 603 pp.

——, 1984: Streamwise vorticity: The origin of updraft rotation in supercell storms. *J. Atmos. Sci.,* **41,** 2991–3006.

Emanuel, K., 1984: Some dynamical aspects of precipitating convection. Appendix. *Dynamics of Mesoscale Weather Systems,* J. B. Klemp, Ed., NCAR Summer Colloquium Notes, 591 pp. [Available from NCAR, P.O. Box 3000, Boulder, CO 80307]

Fujita, T., 1971: Proposed mechanism of suction spots accompanied by tornadoes. *Preprints, Seventh Conf. Severe Local Storms,* Kansas City, Amer. Meteor. Soc., 208–213.

——, and H. Grandoso, 1968: Split of a thunderstorm into anticyclonic and cyclonic storms and their motion as determined from numerical model experiments. *J. Atmos. Sci.,* **25,** 416–439.

Hammond, G. R., 1967: Study of a left moving thunderstorm of 23 April 1964. IERTM-NSSL-31, ESSA, 67 pp.

Klemp, J. B., and R. B. Wilhelmson, 1978a: The simulation of three-dimensional convective storm dynamics. *J. Atmos. Sci.,* **35,** 1070–1096.

——, and ——, 1978b: Simulations of right and left moving storms produced through storm splitting. *J. Atmos. Sci.,* **35,** 1097–1110.

——, and R. Rotunno, 1982: The influence of the shear-induced pressure gradient on thunderstorm motion. *Mon. Wea. Rev.,* **110,** 136–151.

——, and ——, 1983: A case study of the tornadic region within a supercell thunderstorm. *J. Atmos. Sci.,* **40,** 359–377.

——, R. B. Wilhelmson and P. S. Ray, 1981: Observed and numerically simulated structure of a mature supercell thunderstorm. *J. Atmos. Sci.,* **38,** 1558–1580.

Lemon, L. R., and C. A. Doswell, III, 1979: Severe thunderstorm evolution and mesocyclone structure as related to tornadogenesis. *Mon. Wea. Rev.,* **107,** 1184–1197.

Lilly, D. K., 1979: The dynamical structure and evolution of thunderstorms and squall lines. *Ann. Rev. Earth Planet Sci.,* **7,** 117–161.

——, 1982: The development and maintenance of rotation in convective storms. *Topics in Atmospheric and Oceanographic Sciences: Intense Atmospheric Vortices.* L. Bengtsson and J. Lighthill, Eds., Springer-Verlag, Berlin & Heidelberg, 149–182.

——, 1983: Dynamics of rotating thunderstorms. *Mesoscale Meteorology—Theories, Observations, and Models.* D. K. Lilly and T. Gal-Chen, Eds., D. Reidel, Dordrecht, 531–544.

——, 1985: The Structure, Energetics and Propagation of Rotating Convective Storms. Part II: Helicity and Storm Stabilization. *J. Atmos. Sci.,* **42,** 126–140.

Marroquin, A., and D. J. Raymond, 1982: A linearized convective overturning model for prediction of thunderstorm movement. *J. Atmos. Sci.,* **39,** 146–151.

Newton, C. W., and S. Katz, 1958: Movement of large convective rainstorms in relation to winds aloft. *Bull. Amer. Meteor. Soc.,* **39,** 129–136.

Phillips, O. M., 1966: *The Dynamics of the Upper Ocean.* Cambridge University Press, 261 pp.

Rotunno, R., 1981: On the evolution of thunderstorm rotation. *Mon. Wea. Rev.,* **109,** 577–586.

——, and J. B. Klemp, 1982: The influence of the shear-induced pressure gradient on thunderstorm motion. *Mon. Wea. Rev.,* **110,** 136–151.

Schlesinger, R. E., 1978: A three-dimensional numerical model of an isolated thunderstorm. Part I: Comparative experiments for variable ambient wind shear. *J. Atmos. Sci.,* **35,** 690–713.

——, 1980: A three-dimensional numerical model of an isolated thunderstorm. Part II: Dynamics of updraft splitting and mesovortex couplet evolution. *J. Atmos. Sci.,* **37,** 395–420.

——, 1984: Effects of the pressure perturbation field in numerical models of unidirectionally sheared thunderstorm convection: two versus three-dimensions. *J. Atmos. Sci.,* **41,** 1571–1587.

Weisman, M. L., and J. B. Klemp, 1982: The dependence of numerically simulated convective storms on vertical wind shear and buoyancy. *Mon. Wea. Rev.,* **110,** 504–520.

——, and ——, 1984: The structure and classification of numerically simulated convective storms in directionally varying wind shears. *Mon. Wea. Rev.,* **112,** 2479–2498.

Wilhelmson, R. B., and J. B. Klemp, 1978: A numerical study of storm splitting that leads to long-lived storms. *J. Atmos. Sci.,* **35,** 1974–1986.

——, and ——, 1981: A three-dimensional numerical simulation of splitting severe storms on 3 April 1964. *J. Atmos. Sci.,* **38,** 1581–1600.